analytical chemistry

Article

pubs.acs.org/ac

Manipulation of Intraparticle Charge Delocalization by Selective Complexation of Transition-Metal Ions with Histidine Moieties

Xiongwu Kang,[‡] Xiang Li,[†,‡] William M. Hewitt,[‡] Nathaniel B. Zuckerman,[‡] Joseph P. Konopelski,*[,‡] and Shaowei Chen*[,‡]

[‡]Department of Chemistry and Biochemistry, University of California, 1156 High Street, Santa Cruz, California 95064, United States

Supporting Information

ABSTRACT: Ruthenium nanoparticles were cofunctionalized with pyrene and histidine moieties through Ru=carbene π bonds. The selective complexation of the histidine moiety with transition-metal ions led to a marked diminishment of the emission peak at 490 nm which arose from the nanoparticle-bridged pyrene moieties that behaved analogously to pyrene dimers with a conjugated spacer. This is accounted for by the polarization of the core electrons by the added positive charge that impacted the intraparticle charge delocalization between the particle-bound pyrene moieties. This electronic interaction was likely facilitated by the π interactions between the metal ions and the imidazole ring as well as by the conjugated molecular backbone that linked the imidazole ring to the nanoparticle cores. Within the present experimental context, of all the metal ions tested, the impacts were much more drastic with Pb^{2+}, Co^{2+}, and Hg^{2+} than with Li^+, K^+, Rb^+, Mg^{2+}, Ca^{2+}, and Zn^{2+} ions, with the most sensitive variation observed with Pb^{2+}. This is ascribed to the enhanced π interactions of the histidine moiety with the Pb^{2+}, Co^{2+}, and Hg^{2+} ions because of their capability of donating d electrons, a behavior consistent with prior studies based on conventional histidine-metal ion complexes.

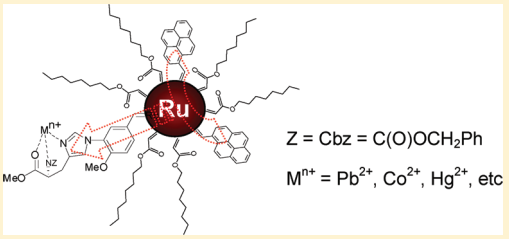

Organically capped transition-metal nanoparticles represent a unique class of nanoscale composite materials where the material properties may be readily manipulated by the chemical nature of the metal cores as well as the structures of the surface organic ligands.[1−4] Recently it has also been found that the metal−ligand interfacial bonding interactions can play a significant role in regulating the nanoparticle optical and electronic properties. For instance, when ferrocenyl moieties are bound onto ruthenium nanoparticle surfaces by ruthenium-carbene (Ru=C) or ruthenium-acetylide (Ru−C≡) bonds, apparent intervalence charge transfer occurs between the particle-bound ferrocenyl groups, as manifested in electrochemical and near-infrared spectroscopic measurements, analogous to conventional ferrocenyl oligomers bridged by conjugated chemical linkers.[5,6] Furthermore, when fluorophores such as pyrene or anthracene moieties are attached onto the nanoparticle surface by similar interfacial linkages, the photoemission profiles resemble those of their dimeric derivatives, again, suggesting effective intraparticle charge delocalization by virtue of the conjugated metal−ligand bonds.[7,8]

Note that the nature of the intraparticle charge transfer through this specific metal−ligand bonding has been ascribed to the effective overlap between the d_π orbital or the $p_\pi d_\pi$ hybrid of the ruthenium metal and the π^* orbital of the ligands,[9,10] as well as to the conducting metal cores of the nanoparticles that serve as the chemical linkage in bridging the functional moieties, as manifested in constrained density functional theory (CDFT) studies.[11,12] Thus, there are at least two aspects that warrant significant attention here. First, as the particle-bound functional moieties behave collectively, electron/energy transfer at part of the surface sites may be propagated and/or amplified throughout the entire nanoparticles, leading to enhanced sensing of the local chemical environment. This has been demonstrated, for instance, by the detection of nitrophenyl compounds with pyrene-functionalized ruthenium nanoparticles.[13] Second, perturbation of the energy of the core electrons may also impact the extent of charge delocalization between the functional moieties on the nanoparticle surface. This has been exemplified by ruthenium nanoparticles functionalized by alkynide derivatives where the extent of conjugation between the particle-bound acetylide moieties can be readily varied by the charge state of the nanoparticle cores.[14] In addition, with the incorporation of crown ether moieties onto the ruthenium nanoparticle surface, the specific binding of certain alkali metal ions leads to apparent polarization of the metal core electrons, as reflected in the variation of the photoluminescence characteristics of the pyrene moieties.[15]

In the present study, we take advantage of the unique characteristics of histidine derivatives in complexation with selective transition-metal ions to extend the study of the manipulation of intraparticle charge delocalization. Histidine moieties have long been known to bind to metal cations, and

Received: December 4, 2011
Accepted: January 20, 2012
Published: January 21, 2012

   dx.doi.org/10.1021/ac203218h | *Anal. Chem.* 2012, 84, 2025−2030

such unique properties have been exploited for protein separation and structural analysis.[16−19] This is largely due to the specific interactions between the imidazole ring and metal ions, where the metal center lies in the ring plane along the lone pair electrons of the N3 nitrogen atom,[20] involving largely π-type (rather than σ bonding) interactions between the ligand and metal ions since imidazole is a good π-electron acceptor.[16] Apparently such bonding interactions may be strengthened by metal ions with increasing capability of donating d electrons.

Experimentally, ruthenium nanoparticles will be cofunctionalized with vinylpyrene and a vinylbenzohistidine derivative, both of which are bound onto the nanoparticle surface by ruthenium-carbene (Ru═C) π bonds. The complexation of selective metal ions with the histidine ligands is anticipated to induce polarization of the ruthenium metal core electrons, leading to deliberate manipulation of intraparticle extended conjugation between the particle-bound pyrene moieties and hence the photoluminescence characteristics, thanks to the π molecular backbone that bridges the imidazole ring to the nanoparticle core. The experimental results show that whereas virtually no change appears in the nanoparticle photoluminescence upon the addition of alkali or alkali-earth metal ions (e.g., Li^+, K^+, Rb^+, Mg^{2+}, and Ca^{2+}, or Zn^{2+}), apparent differences are observed with Hg^{2+}, Co^{2+}, and Pb^{2+} ions. Additionally, within the present experimental context, the nanoparticle photoluminescence exhibits the most drastic variation in the presence of Pb^{2+} ions. Such differentiation and selectivity toward transition-metal ions may be exploited for the sensitive chemical detection and analysis.

EXPERIMENTAL SECTION

Chemicals. Ruthenium chloride ($RuCl_3$, 99+%, ACROS), 1,2-propanediol (ACROS), sodium acetate trihydrate ($NaOAc{\cdot}3H_2O$, MC&B), lithium perchlorate ($LiClO_4$, 99.5%, Fisher Chemical), sodium perchlorate ($NaClO_4$, Fisher Chemical), potassium perchlorate ($KClO_4$, Fisher Chemical), rubidium perchlorate ($RbClO_4$, Fisher Chemical), magnesium perchlorate ($Mg(ClO_4)_2$, Aldrich Chemical), calcium perchlorate ($Ca(ClO_4)_2$, Aldrich Chemical), lead(II) perchlorate ($Pb(ClO_4)_2$, ACROS), cobalt(II) perchlorate ($Co(ClO_4)_2$, Aldrich), mercuric perchlorate ($Hg(ClO_4)_2$, Aldrich), and extra dry N,N-dimethylformamide (DMF, 99.8%, Aldrich) were all used as received. Water was supplied by a Barnstead Nanopure water system (18.3 MΩ·cm).

Synthesis of Functional Ligands. Standard syringe techniques using flame and/or oven-dried glassware were utilized for syntheses under an atmosphere of dry nitrogen. All melting points are uncorrected. Proton NMR spectra were acquired in the specified deuterated solvents at 500 MHz, while carbon NMR at 125 MHz. The chemical shifts are reported in parts per million (ppm), and ^1H and ^{13}C spectra were calibrated against residual solvent peaks as follows: $CDCl_3$ (δ = 7.26, 77.2). Anhydrous THF and CH_2Cl_2 were obtained from a solvent purification system. All other solvents and reagents were used as received unless otherwise noted.

The synthesis of octyl diazoacetate (ODA), 1-vinylpyrene, and 1-allylpyrene has been described previously.[7] The vinylbenzohistidine ligand **5** for metal ion chelation was synthesized from *p*-methoxybenzaldehyde **1** by iodination following a published method as outlined in Scheme 1 (details in the Supporting Information).[21] The resultant iodobenzaldehyde **2** was subjected to Wittig olefination to afford desired terminal alkene **3** in 59% yield. Transformation to the corresponding

Scheme 1. Synthetic Procedure of Metal-Ion Chelating Ligand 5

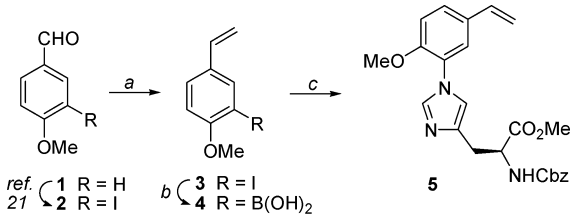

a) $Ph_3P{=}CH_2$, 59%; *b*) *n*-BuLi, $B(O\text{-}i\text{-}Pr)_3$, 57%; *c*) Z-His-OMe, cat. $[Cu(OH)TMEDA]_2Cl_2$, 39%

boronic acid **4** proceeded in 57% isolated yield and became the coupling partner to Z-His-OMe via Collman's protocol,[22] yielding the target compound **5** for selective ion binding.[23]

Functionalization of Ruthenium Nanoparticles. The preparation of carbene-stabilized ruthenium nanoparticles has been detailed previously.[7,24] Experimentally, ruthenium colloids, which exhibited a core diameter of 2.12 ± 0.72 nm as determined by transmission electron microscopy measurements (Figure S1 in the Supporting Information), were prepared by thermolytic reduction of $RuCl_3$ in 1,2-propanediol at controlled temperatures and then mixed with octyl diazoacetate (ODA), affording carbene-stabilized ruthenium (Ru═C8) nanoparticles. The nanoparticles were then functionalized by olefin metathesis reactions with a mixture of compound **5** and 1-vinylpyrene (Scheme 2) where the histidine and pyrene moieties were both incorporated into the nanoparticle protecting monolayer. The resulting particles were denoted as Ru═VPyHis. The concentrations of the pyrene, histidine, and ODA ligands on the ruthenium nanoparticle surface were quantified by ^1H NMR measurements where the organic components were extracted after the ruthenium cores were dissolved by dilute KCN (Figure S2). Based on the integrated peak areas of the protons for pyrene (8.4 to 7.8 ppm), phenyl ring (7.37 to 7.27 ppm), imidazole ring (7.68 ppm and 6.99 ppm), and methyl protons (0.9 ppm), the surface coverage was estimated to be 5.3%, 10.5%, and 84.2%, for the pyrene, benzohistidine (**5**), and the original ODA ligands, respectively.

Spectroscopy. UV−vis spectroscopic studies were performed with an ATI Unicam UV4 spectrometer by using a 1-cm quartz cuvette with a resolution of 2 nm. Fluorescence spectra were acquired with a PTI fluorescence spectrometer by using the same solutions for UV−vis measurements. In a typical measurement, 3 mL of a Ru═VPyHis nanoparticle solution at a concentration of 0.015 mg/mL in DMF was added to a quartz cuvette. A calculated amount of a metal salt analyte (0.05 M in DMF) was then injected into the cuvette by a Hamilton microliter syringe. Fluorescence spectra were collected after thorough mixing of the analyte with the nanoparticle solution.

RESULTS AND DISCUSSION

As mentioned earlier, the incorporation of both the pyrene and benzohistidine (**5**) ligands onto the Ru═C8 nanoparticle surface has been confirmed by ^1H NMR measurements, and their spectroscopic signatures have been used to quantify their respective surface concentrations (vide ante). The presence of the pyrene moieties on the nanoparticle surface is further manifested in UV−vis absorption measurements, as depicted in Figure 1. One can see that the Ru═VPyHis nanoparticles (red dashed curve) exhibited an exponential decay profile which is ascribed to Mie scattering of the nanosized Ru metal cores.[25]

dx.doi.org/10.1021/ac203218h | *Anal. Chem.* 2012, 84, 2025−2030

Scheme 2. Functionalization of Carbene-Stabilized Ruthenium (Ru═C8) Nanoparticles with Vinyl-Terminated Functional Ligands through Olefin Metathesis Reactions, Where the Resulting Nanoparticles May Exhibit Specific Complexation with Transition-Metal Ions (M^{n+})

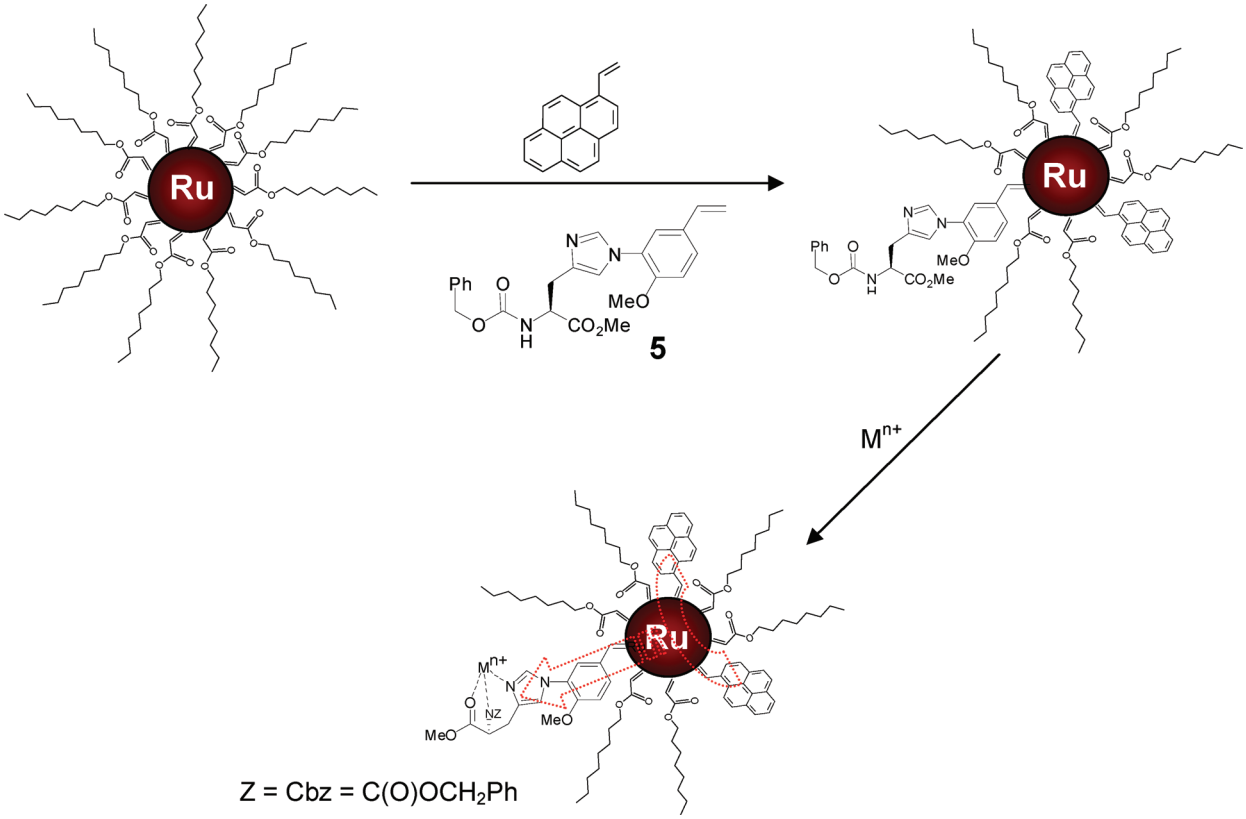

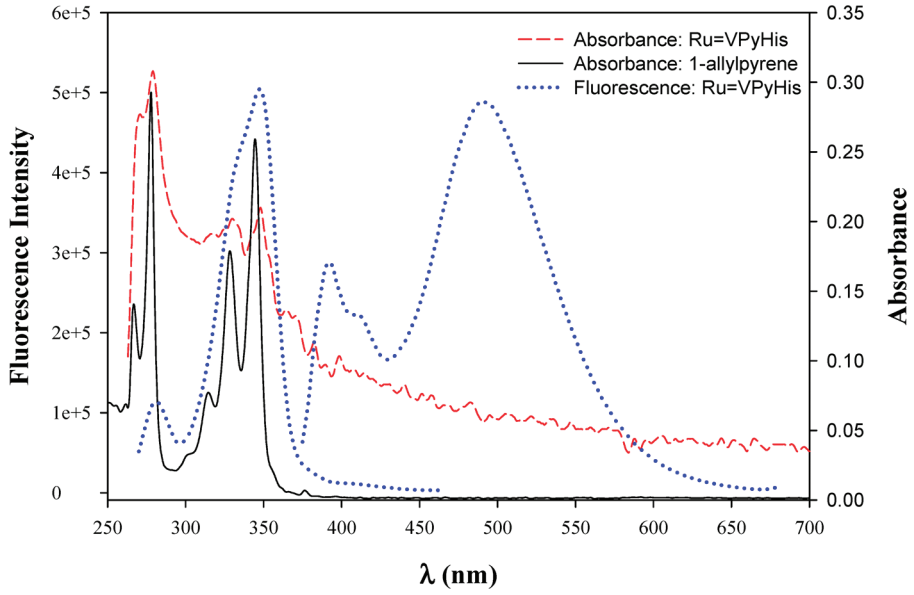

Figure 1. UV−vis absorption (dashed curve) and fluorescence (excitation and emission, dotted curves) spectra of Ru═VPyHis nanoparticles (0.015 mg/mL in DMF). The absorption spectrum (solid curve) of 1-allylpyrene (0.1 mM in DMF) is also included.

Additionally, four major absorption peaks can be identified at 345 nm, 330 nm, 280 nm, and 270 nm. These are consistent with those of monomeric pyrene, as exemplified by 1-allylpyrene (black solid curve), signifying the successful attachment of the pyrene moieties onto the nanoparticle surface by olefin metathesis reactions (Scheme 2). Furthermore, the excitation and emission spectra of the nanoparticles (blue dotted curves) are consistent with those obserbed previously with 1-vinylpyrene-functionalized ruthenium (Ru═VPy) nanoparticles.[7] The key features include a major emission peak centered at 490 nm and two minor ones at 390 and 413 nm, with a major excitation peak at 350 nm. The emission peak at 490 nm is ascribed to the charge delocalization between the particle-bound pyrene moieties such that they behave

dx.doi.org/10.1021/ac203218h | *Anal. Chem.* 2012, 84, 2025−2030

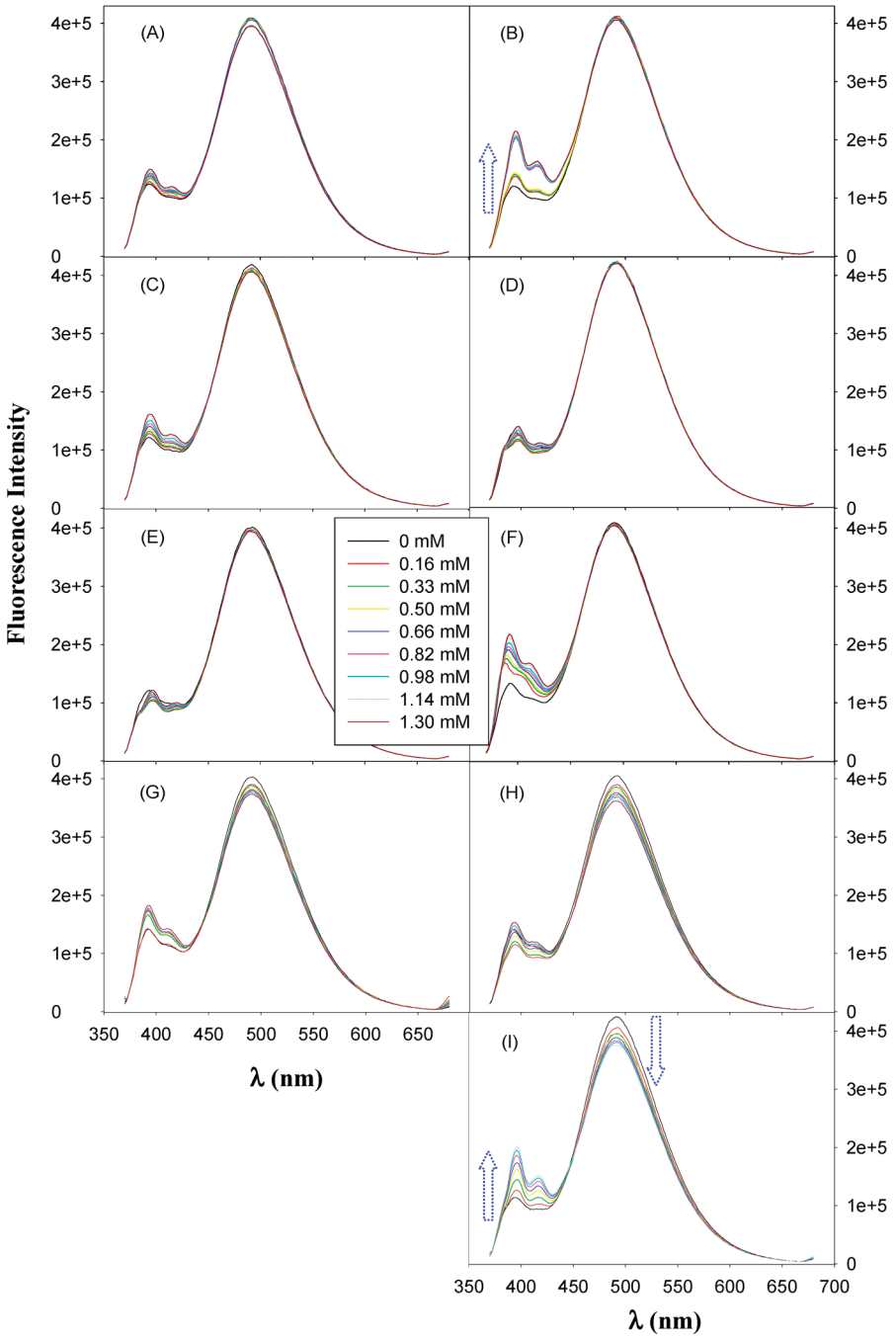

Figure 2. Emission spectra of Ru═VPyHis nanoparticles (0.015 mg/mL in DMF) with the addition of (A) Li^+, (B) K^+, (C) Rb^+, (D) Mg^{2+}, (E) Ca^{2+}, (F) Zn^{2+}, (G) Hg^{2+}, (H) Co^{2+}, and (I) Pb^{2+} at different concentrations (specified in figure legends). The excitation wavelength is all set at 350 nm.

analogously to dimeric pyrene with a conjugated spacer, whereas those ones at 390 and 413 nm are consistent with monomeric pyrene.[7]

The variation of these fluorescence signatures upon the addition of metal ions will then be examined and exploited for their detection and analysis. It is anticipated that the complexation of the imidazole moiety with metal ions incorporates positive charges into the nanoparticle surface layer, which may then polarize the core electrons and hence impact the intraparticle charge delocalization between the pyrene moieties. Scheme 2 depicts a possible structure of the metal-histidine complex, where the nitrogen (N3) atom in the imidazole ring, along with the nitrogen and oxygen atoms of the carboxylate moieties plays a significant role in the complexation with metal ions. This is built upon ^{1}H NMR studies of the interactions between a benzohistidine derivative (similar to **5**, Figure S3) and $Pb(ClO_4)_2$ carried out in the Konopelski group.[26] Notably, the chemical shift of the C2 proton in the imidazole ring shows an apparent increase (ca. 0.5 ppm) with the increase of the Pb^{2+} concentration up to a Pb^{2+}:ligand ratio of 1.75:1, whereas concurrently the methyl protons of the methyl carboxylate motif exhibit an abrupt decrease from 3.77 to 3.38 at the Pb^{2+}:ligand ratio of 1:1, suggesting specific binding of Pb^{2+} ions with the imidazole moiety and the ester

dx.doi.org/10.1021/ac203218h | *Anal. Chem.* 2012, 84, 2025−2030

oxygen. The proposed structure of the metal-histidine complex in Scheme 2 is also consistent with literature studies of the coordination chemistry of Cd^{2+}, Pb^{2+}, and Hg^{2+} with triazole derivatives.[27,28] In the present study, because of the aromaticity in the imidazole ring[16] and hence the conjugated molecular backbone that bridges the metal center to the metal core, the nanoparticle core electrons will most likely be polarized (Scheme 2). This will then impact the intraparticle charge delocalization between the particle-bound pyrene moieties, leading to a diminishment of the emission at 490 nm and concurrently an enhancement at 390 nm.[15] In fact, this is what we observed in experimental measurements.

Figure 2 shows the fluorescence emission spectra of the Ru═VPyHis nanoparticles (0.015 mg/mL in DMF) with the addition of different concentrations (up to 1.30 mM) of (A) Li^+, (B) K^+, (C) Rb^+, (D) Mg^{2+}, (E) Ca^{2+}, (F) Zn^{2+}, (G) Hg^{2+}, (H) Co^{2+}, and (I) Pb^{2+}, which were specified in the figure legends. The excitation wavelength was all set at 350 nm. It can be seen that in the presence of Hg^{2+}, Co^{2+}, and Pb^{2+} ions, the emission peak intensity at 490 nm shows an apparent decrease with increasing ion concentrations, as depicted in panels (G) − (I); whereas the addition of Li^+, K^+, Rb^+, Mg^{2+}, Ca^{2+}, and Zn^{2+} ions led to almost no change of the emission characteristics at 490 nm, as manifesred in panels (A) to (F). This is most likely due to the specific complexation of the imidazole moiety with the Hg^{2+}, Co^{2+}, and Pb^{2+} ions (Scheme 2), where the added positive charge into the nanoparticle protecting layer led to polarization of the particle core electrons. This electronic interaction is likely facilitated by the π interactions between the metal ion centers and the imidazole ring as well as by the conjugated molecular backbone that bridges the imidazole ring to the Ru core (Scheme 2), leading to a diminishment of the intraparticle charge delocalization between the particle-bound pyrene moieties. Consequently, the pyrene moieties exhibited increasingly monomeric characters, as manifested in the concurrent increase of the emission intensity at 390 nm (more discussion below). Similar variation of the nanoparticle fluorescence has been observed with ruthenium nanoparticles cofunctionalized by vinylpyrene and vinylbenzo(crown ether) ligands, where the binding of the crown ether moieties with selected alkaline metal ions led to an apparent diminishment of the emission intensity at 490 nm.[29]

In contrast, no such complexation was formed between the histidine moiety and the ions of Li^+, K^+, Rb^+, Mg^{2+}, Ca^{2+}, and Zn^{2+}, and the emission intensity at 490 nm remained virtually unchanged, suggestive of no impact on the intraparticle charge delocalization between the particle-bound pyrene moieties, most probably because of the lack of π interactions between the metal ions and the imidazole moiety. Nevertheless, one may note that the emission intensity at 390 nm also depicts an increase with the addition of these ions (up to 1.30 mM), in particular with (B) K^+ and (F) Zn^{2+}. This is most likely due to the enhanced fluorescence of the benzoimidazole moieties with the addition of the metal ions. In fact, as depicted in Figure S4, one can see that the monomeric compound **5** exhibited a well-defined emission peak at 340 nm and two excitation peaks at 275 and 302 nm, consistent with the fluorescence characteristics of benzoimidazole derivatives.[30] Upon the addition of K^+, Zn^{2+}, and Pb^{2+} ions, the emission intensity exhibited an apparent increase. More importantly, when excited at 350 nm (same as that for the Ru═VPyHis nanoparticles, Figure 2), the solution showed a somewhat broad emission peak between 370 and 450 nm, and the intensity of this emission feature increased with increasing ion concentration. This happens to overlap with the emission peak around 390 nm of the Ru═VPyHis nanoparticles (Figure 2). Therefore, the enhanced emission around 390 nm observed with the Ru═VPyHis nanoparticles upon the addition of varied metal ions might be ascribed to one or both of the following two factors: ion-induced enhancement of the fluorescence of the benzoimidazole moiety (as in the case of Li^+, K^+, Rb^+, Mg^{2+}, Ca^{2+}, and Zn^{2+} ions) and reduced intraparticle charge delocalization between the particle-bound pyrene moieties (as in the case of Hg^{2+}, Co^{2+}, and Pb^{2+} ions).

Figure 3 shows the variation of the peak intensity at 490 nm with the concentrations of the added ions, which is all

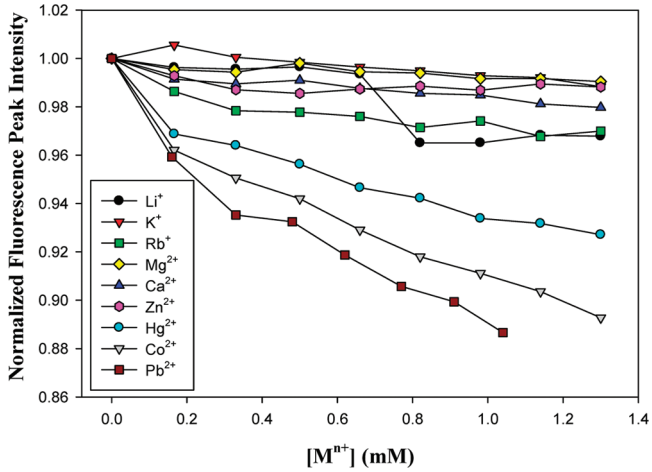

Figure 3. Variation of the Ru═VPyHis nanoparticle fluorescence intensity at 490 nm with the addition of varied metal ions, which was normalized to that prior to the addition of the respective metal ions. Symbols are experimental data acquired from Figure 2, and lines are for eye-guiding only.

normalized to that prior to the addition of the respective ions. Rather marked diminishment of the nanoparticle photoluminescence can be observed with the addition of Pb^{2+}, Co^{2+}, and Hg^{2+} ions, whereas the photoemission intensity remains virtually unchanged with other ions.

For instance, with the addition of 1 mM of Pb^{2+}, Co^{2+}, and Hg^{2+} ions, the emission intensity decreases by 11%, 9%, and 6.5%, respectively; whereas for the Li^+, K^+, Rb^+, Mg^{2+}, Ca^{2+}, and Zn^{2+} ions, the impacts are minimal with the diminishment of the emission intensity less than 2%. In other words, within the present experimental context, Pb^{2+} exhibits the most drastic impacts on the nanoparticle fluorescence at 490 nm among the nine ions tested. These experimental results suggest much stronger complexation of the histidine moiety with the Pb^{2+}, Co^{2+}, and Hg^{2+} ions than with alkaline and alkaline-earth metal ions. This may be accounted for by the enhanced π interactions between the ligand and the former group of metal ions because of their capability of donating d electrons.[16] Interestingly, Zn^{2+} behaved analogously to the alkaline and alkaline-earth ions, although the formation of stable zinc-imidazole complexes has long been known with simple molecular ligands.[16] This is most probably because the zinc-imidazole complexes typically adopt a distorted octahedral configuration, which is sterically unfavorable on the nanoparticle surface due to the tight packing of the capping ligands.

Note that the strength of ion complexation is highly dependent on a variety of structural parameters, such as

dx.doi.org/10.1021/ac203218h | *Anal. Chem.* 2012, 84, 2025−2030

metal−ligand bond length,[31,32] metal−ligand bond geometries,[33] and coordination number[34] as well as oxidation state and ionic bonding effect.[35] For instance, the role of carboxylate moiety in the complexation with metal ions has been recognized and discussed previously.[35] The spin state and Jahn−Teller effect might also play a role in the complexation of histidine and transition-metal ions, as observed in iron complexes.[36] Such unique chemistry may be exploited for further manipulation of the nanoparticle optical/electronic properties as well as for selective sensing of metal ions by deliberate functionalization of the nanoparticle surface. These will be pursued in future work.

CONCLUSION

In this study, ruthenium nanoparticles were cofunctionalized with pyrene and histidine moieties by Ru=carbene π bonds. Specific complexation of the histidine moiety with selected metal ions was exploited as an effective mechanism to manipulate the intraparticle charge delocalization between the particle-bound pyrene moieties, where the added positive charge into the particle surface layer led to effective polarization of the particle core electrons. Within the present experimental context, Pb^{2+}, Co^{2+}, and Hg^{2+} ions exhibited much more significant impacts than alkaline and alkaline-earth ions (Li^{+}, K^{+}, Rb^{+}, Mg^{2+}, Ca^{2+}, and Zn^{2+}) on the diminishment of the nanoparticle fluorescence at 490 nm, suggesting a decreasing order of complexation strength with the histidine moieties. Importantly, Pb^{2+} stood out with the most drastic variation. This is attributed to the enhanced π interactions between the imidazole moiety with metal ions that are more likely to donate d electrons. The results are consistent with prior literature reports based on conventional metal ion-histidine complexes.

ASSOCIATED CONTENT

Supporting Information

Synthetic details of ligand **5**, TEM micrograph of ruthenium nanoparticles, proton NMR spectrum of the Ru=VPyHis nanoparticles where the organic components were collected after the metallic cores were dissolved in dilute KCN, molecular structructure of a benzohistidine derivative and the variation of the chemical shifts of selected protons in Pb^{2+} ion titration measurements, and fluorescence spectra of vinylbenzohistidine ligand **5** with the addition of varied metal ions. This material is available free of charge via the Internet at http://pubs.acs.org.

AUTHOR INFORMATION

Corresponding Author

*E-mail: joek@ucsc.edu (J.K.); shaowei@ucsc.edu (S.C.).

Present Address

[†]School of Chemistry and Chemical Engineering, Nanjing University, Nanjing, Jiangsu 210093, P. R. China.

Notes

The authors declare no competing financial interest.

ACKNOWLEDGMENTS

This work was supported, in part, by the National Science Foundation through grants CHE-1012256 and CHE-0832605 as well as by the ACS-Petroleum Research Fund (49137-ND10). TEM studies were carried out at the National Center for Electron Microscopy, Lawrence Berkeley National Laboratory which is supported by the US Department of Energy.

REFERENCES

(1) Brust, M.; Walker, M.; Bethell, D.; Schiffrin, D. J.; Whyman, R. *J. Chem. Soc., Chem. Commun.* **1994**, 801−802.

(2) Whetten, R. L.; Shafigullin, M. N.; Khoury, J. T.; Schaaff, T. G.; Vezmar, I.; Alvarez, M. M.; Wilkinson, A. *Acc. Chem. Res.* **1999**, *32*, 397−406.

(3) Templeton, A. C.; Wuelfing, M. P.; Murray, R. W. *Acc. Chem. Res.* **2000**, *33*, 27−36.

(4) Shenhar, R.; Rotello, V. M. *Acc. Chem. Res.* **2003**, *36*, 549−561.

(5) Chen, W.; Chen, S. W.; Ding, F. Z.; Wang, H. B.; Brown, L. E.; Konopelski, J. P. *J. Am. Chem. Soc.* **2008**, *130*, 12156−12162.

(6) Chen, W.; Zuckerman, N. B.; Kang, X. W.; Ghosh, D.; Konopelski, J. P.; Chen, S. W. *J. Phys. Chem. C* **2010**, *114*, 18146−18152.

(7) Chen, W.; Zuckerman, N. B.; Lewis, J. W.; Konopelski, J. P.; Chen, S. W. *J. Phys. Chem. C* **2009**, *113*, 16988−16995.

(8) Chen, W.; Pradhan, S.; Chen, S. W. *Nanoscale* **2011**, *3*, 2294−2300.

(9) Pruchnik, F. P. *Organometallic chemistry of the transition elements*; Plenum Press: New York, 1990.

(10) Tsutsui, M.; Courtney, A. *Adv. Organomet. Chem.* **1977**, *16*, 241−282.

(11) Ding, F. Z.; Wang, H. B.; Wu, Q.; Van Voorhis, T.; Chen, S. W.; Konopelski, J. P. *J. Phys. Chem. A* **2010**, *114*, 6039−6046.

(12) Ding, F. Z.; Chen, S. W.; Wang, H. B. *Materials* **2010**, *3*, 2668−2683.

(13) Chen, W.; Zuckerman, N. B.; Konopelski, J. P.; Chen, S. W. *Anal. Chem.* **2010**, *82*, 461−465.

(14) Kang, X. W.; Zuckerman, N. B.; Konopelski, J. P.; Chen, S. W. *Angew. Chem., Int. Ed.* **2010**, *49*, 9496−9499.

(15) Kang, X. W.; Chen, W.; Zuckerman, N. B.; Konopelski, J. P.; Chen, S. W. *Langmuir* **2011**, *27*, 12636−12641.

(16) Sundberg, R. J.; Martin, R. B. *Chem. Rev.* **1974**, *74*, 471−517.

(17) Hemdan, E. S.; Zhao, Y. J.; Sulkowski, E.; Porath, J. *Proc. Natl. Acad. Sci. U.S.A.* **1989**, *86*, 1811−1815.

(18) Regan, L. *Annu. Rev. Biophys. Biomol. Struct.* **1993**, *22*, 257−281.

(19) Zoroddu, M. A.; Kowalik-Jankowska, T.; Kozlowski, H.; Molinari, H.; Salnikow, K.; Broday, L.; Costa, M. *Biochim. Biophys. Acta* **2000**, *1475*, 163−168.

(20) Chakrabarti, P. *Protein Eng.* **1990**, *4*, 57−63.

(21) Hathaway, B. A.; White, K. L.; McGill, M. E. *Synth. Commun.* **2007**, *37*, 3855−3860.

(22) Collman, J. P.; Zhong, M. *Org. Lett.* **2000**, *2*, 1233−1236.

(23) Mahoney, M. E.; Oliver, A.; Emarsdottir, O.; Konopelski, J. P. *J. Org. Chem.* **2009**, *74*, 8212−8218.

(24) Chen, W.; Davies, J. R.; Ghosh, D.; Tong, M. C.; Konopelski, J. P.; Chen, S. W. *Chem. Mater.* **2006**, *18*, 5253−5259.

(25) Creighton, J. A.; Eadon, D. G. *J. Chem. Soc,. Faraday Trans.* **1991**, *87*, 3881−3891.

(26) Landaverry, Y. R. Ph.D. Dissertation, University of California, Santa Cruz, CA, 2007.

(27) Ambrosi, G.; Formica, M.; Fusi, V.; Giorgi, L.; Macedi, E.; Micheloni, M.; Pontellini, R. *Inorg. Chim. Acta* **2009**, *362*, 3709−3714.

(28) Liu, K.; Shi, W.; Cheng, P. *Dalton Trans.* **2011**, *40*, 8475−8490.

(29) Kang, X. W.; Chen, W.; Zuckerman, N. B.; Konopelski, J. P.; Chen, S. W. *Langmuir* **2011**, *27*, 12636.

(30) Feng, K.; Hsu, F. L.; Van DerVeer, D.; Bota, K.; Bu, X. R. *J. Photochem. Photobiol., A* **2004**, *165*, 223−228.

(31) Orpen, A. G.; Brammer, L.; Allen, F. H.; Kennard, O.; Watson, D. G.; Taylor, R. *J. Chem. Soc., Dalton Trans.* **1989**, S1−S83.

(32) Allen, F. H.; Kennard, O.; Watson, D. G.; Brammer, L.; Orpen, A. G.; Taylor, R. *J. Chem. Soc., Perkin Trans. 2* **1987**, S1−S19.

(33) Harding, M. M. *Acta Crystallogr., Sect. D: Biol. Crystallogr.* **2002**, *58*, 872−874.

(34) See, R. F.; Kruse, R. A.; Strub, W. M. *Inorg. Chem.* **1998**, *37*, 5369−5375.

(35) Hocking, R. K.; Hambley, T. W. *Dalton Trans.* **2005**, 969−978.

(36) Gutlich, P.; Garcia, Y.; Goodwin, H. A. *Chem. Soc. Rev.* **2000**, *29*, 419−427.